



Aqueous oxidation of coal-associated pyrite and standard pyrite mineral towards understanding the depyritization kinetics and acid formations

Angana Mahanta^{1,2} · Binud Attry¹ · Binoy K. Saikia^{1,2} 

Received: 14 February 2024 / Revised: 20 May 2024 / Accepted: 10 September 2024
© The Author(s) 2024

Abstract

In coal mining areas, the ambient atmospheric and aqueous oxidation of pyrite minerals (FeS_2) associated with coal as well as the other accompanying strata is significant in understanding the extent of acid mine drainage (AMD), the cause of severe environmental pollution. Therefore, in this paper, the oxidation kinetics of the coal-associated pyrite (CAPy) present in a coal sample (TpHM1) has been studied via aqueous leaching depyritization experiments at variety of temperatures and time intervals without the incorporation of any oxidizer. The outcomes obtained are juxtaposed with the standard pyrite mineral (SPM) oxidation at the same experimental conditions. Also, the coal and SPM slurry residues and filtrates obtained after aqueous leaching at 25 °C and 90 °C for 0 h and 24 h, respectively, were extensively analyzed through high-resolution transmission electron microscopy (HR-TEM), Powder X-ray diffraction (P-XRD), and X-ray-photoelectron spectroscopy (XPS) for evaluation of the mineralogical composition and proportions of iron and sulfur components during progression of the oxidation reaction. Both the reactions obey pseudo first-order kinetics during pyrite (FeS_2) oxidation but a significant difference in the experimentally found activation energies (E_a) and rate constants (k) values of oxidation kinetics of both CAPy and SPM may be attributed to the varied geochemical compositions of the coal associated pyrite (CAPy). The rate constant for CAPy is much greater than that of SPM implying a higher E_a around 10.838 kJ/mol for SPM as compared to 1.941 kJ/mol for CAPy. The CAPy in coal (TpHM1) is more susceptible to atmospheric oxidation than that of SPM, leading to the formation of acid mine drainage with lower pH. In this paper, the pH values on the basis of stoichiometric pyrite oxidation reaction were calculated and compared with the pH values obtained after aqueous leaching of CAPy to interpret the extent of acid formation and pyrite dissolution. Hence, with the assistance of the current study, further studies on the effects of mineral impurities, whereabouts of pyrite minerals in coal seams, the significance of compositional differences in the CAPy, the effect of metal oxides, and the role of alkalinity producing neutralizing agents of coal in the oxidative dissolution process of pyrite can be investigated.

Keywords Coal pyrite · Oxidation of pyrite · Aqueous leaching of coal · Acid mine drainage · Kinetics of pyrite oxidation

1 Introduction

The economic growth of India is significantly influenced by coal mining enterprises, which additionally contribute to meet the constantly increasing energy needs of several

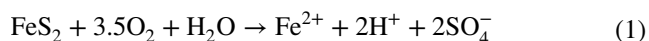
industries, including the power and fertilizer sectors, paper and textile manufacturing, etc. However, coal-mining activities influence the forest, aquatic environment, atmosphere, and habitats for wildlife adjacent to the mining zone. More than 95% of the sulfides found on Earth's surface have been identified in sediments, where they mostly acquire the form of pyrite (Rickard et al. 2017). Pyrite is pervasive in both terrestrial and aquatic habitats and is vital to iron redox cycling (Tabelin et al. 2017). In terms of the environment, pyrite is significant because of its direct impact on the development of acid mine drainage (AMD). India has third largest coal resources in the world and its northeast part contains low-ash, low-rank Cenozoic coal deposits with high

✉ Binoy K. Saikia
bksaikia@gmail.com; bksaikia@neist.res.in

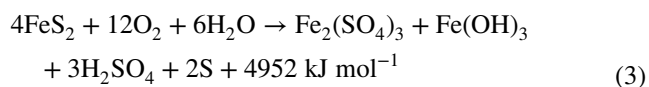
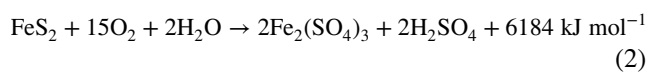
¹ Coal and Energy Division, CSIR-North East Institute of Science and Technology, Jorhat, Assam 785006, India

² Academy of Scientific and Innovative Research (AcSIR), Ghaziabad 201002, India

levels of sulfur and various potentially dangerous organic and mineral-bound elements (Saikia et al. 2015). Coal mining is conducive to a discharge of mine waste, dust, land subsidence, deforestation, spontaneous coal combustion, etc. When exposed to the environment, pyrite (FeS_2) undergoes oxidation due to natural processes or anthropogenic activities, forming sulfuric acid in the presence of humidity (Equeenuddin 2010). The formation and movement of this highly acidic water is called AMD (Saikia et al. 2016). Thus, coal mining activity in the northeastern coalfield, Margherita (northeast India) has caused noteworthy ecological degradation surrounding the mining area and has left an indelible mark on the landscape and ecosystem. This activity cannot only burn up coal resources and bring about staggering economic harm but also produce harmful gases and seriously pollute the environmental conditions (Baruah and Khare 2010; Dutta et al. 2017). Pyrite oxidation in the presence of water and air (ambient condition), leading to the formation of acid (H^+), sulfates (SO_4^{2-}), and aqueous Fe (II) ions:



To comprehend the kinetics and process by which pyrite is transformed into the AMD products in an aqueous media, numerous studies have been carried out (Saikia et al. 2015). The spontaneous combustion of coal mine waste is a global environmental hazard. Sulfurous iron ore and low-heating value coal oxidize during the oxidation stage in compliance with the following reactions (Liu et al. 1998).



These reactions involve in the release of significant quantity of heat exchanges during the atmospheric oxidation stage. Although pyrite is immune to both acidic and alkaline attacks, it dissolves relatively quickly when exposed to oxidants like O_2 and Fe^{3+} through an electrochemical process.

Since, heavy metals and poisonous metalloids are known to be embedded in the crystal structure of natural pyrite (Abraitis et al. 2004), so AMD also includes potentially dangerous elements due to its dissolution in water. A variety of kinds of pyrite, including nodular, layered, fissure filling, and aggregated are enormous, typically occur in coal seams (Ma et al. 2022). The self-thermal oxidation property of pyrite results in the production of ferric sulphate and ferrous sulfate, which enhances the pore structures and surface area of coal in proximity with oxygen. Pyrite's rate of oxidation is influenced by a number of factors, such as oxidant (Fe^{3+} or O_2), pH, redox potential, etc. Due to the metabolism of certain acidophilic bacteria as *Thiobacillus ferrooxidans*, pyrite

encountered in coal is leached to generate acidic drainage (Baruah and Khare 2010). Microorganisms oxidize pyrite at a rate that is several, even hundreds of times quicker than that produced by normal chemical oxidation (Ma et al. 2023). The interaction of metal oxides like hematite and alumina with pyrite and how they impact the general dynamics of pyrite oxidation in nature is one of the significant, but sometimes disregarded phenomenon. Some, previously addressed subjects mostly emphasize on the consequences of metal ions produced from these oxides during dissolution, such as Fe^{3+} , Fe^{2+} , Mn^{2+} , and Al^{3+} (Aller and Rude 1988). Reports say that the coal's depositional environment also impacts the abundance of pyrite and its size distribution (Ma et al. 2022). While fine-grained pyrite has a partially varied occurrence state, including framboidal, euhedral crystalline, spherical, fine-grained agglomerated; etc. Coarse-particle pyrite is mostly abundant in agglomerated, nodular, and fracture-filling forms. The fine-grained pyrite nonetheless has the potential to develop a sophisticated symbiotic connection with the coal matrix (Wang et al. 2016). In conclusion, oxidants (Fe^{3+} and O_2) and bacteria found in coal seams participate in the oxidation process of naturally occurring pyrite, making it far more intricate than the standard mineral pyrite system. However, the majority of earlier investigations (Chen and Chen 1986; Zhao et al. 2022) employed mineral-pyrite for model examinations of pyrite oxidation. The formation conditions and composition of coal-pyrite and mineral-pyrite differ in particular instances, which may render it challenging to extrapolate experimental findings. In this study, two representative samples consisting of raw coal (TpHM1) and grains of standard pyrite mineral (SPM) were subjected to study the oxidation experiments of the intrinsic pyrite present in coal (TpHM1) and SPM sample in order to compare their depyritization kinetics in a controlled atmospheric environment. The chemical and nano-mineralogical makeup of processed coal (TpHM1) and SPM samples, alongside other rate-influencing parameters, were correlated to comprehend precisely why the reaction processes of coal-assisted pyrite (CAPy) and SPM diverge from one another. Furthermore, a comparison of the theoretically calculated pH value and the experimental pH value, on following the aqueous atmospheric oxidation of coal (TpHM1) was assessed for correlation between the two oxidation conditions. In order to gain insight into the oxidation properties of pyrite in coal seams and eventually to cut back on coal spontaneous combustion, the difference in the reaction processes between coal pyrite and mineral pyrite, as well as the influencing elements, were analyzed. Thus, this study will be immensely helpful in comprehending the pyrite dissolving or depyritization kinetics process towards the regulation of acid mine drainage and coal spontaneous combustion.

2 Methods and materials

2.1 Raw coal and standard pyrite mineral samples

The raw coal sample (TpHM1) was collected from the Makum coalfield, Margherita (northeast India) and the standard pyrite mineral (SPM) was purchased from AlfaA-sear (specific gravity 5 g/cm³, hardness 6.5 Mohs scale, and molecular weight of 119.965 g/mol). The raw coal samples were collected in sealed polythene bags and stored in sealed HDPE plastic bottle to avoid any air contact with proper labelling. The acids and reagents used for this study were of analytical grade reagents. The standard pyrite mineral (SPM) sample was composed of Fe and S with no other major trace elements as mentioned. Pyrite mineral sample was first crushed manually using a hammer. The sample was then crushed further to a size of 2–30 mm using a jaw crusher and classified into different particle sizes with distinct crystal grains using a series of sieves.

The selected coal sample (TpHM1) was also pulverized to a size of 2–30 mm using a jaw crusher and then to sizes of <0.5 mm using Rotor Beater Mill. Then, crushed coal samples were processed with a series of sieves into different particle sizes. A particle size less than 212 μm was used for both the processed samples of TPHM1 and SPM.

2.2 Aqueous leaching of samples (depyritisation experiment)

In order to investigate the kinetics of pyrite oxidation in atmospheric conditions, 5 g of both the samples (coal and SPM) were taken in two beakers separately and mixed with 100 ml of distilled water. The solutions in the beaker were then constantly stirred by a magnetic stirrer at about 300 rpm. The stirring experiments were conducted for 0, 0.5, 1, 6, 8, and 24 h (overnight) at the temperature of 25, 50, 75, and 90 °C, respectively, separately for both the samples. The obtained slurry was then filtered to separate the solid phase from the filtrate with a Whatmann-41 filter paper. The filtrates as well as the residues were stored for further analysis.

2.3 Physico-chemical analysis of the aqueous leachates

The aqueous leachates (filtrates) obtained from both the coal and SPM samples after the leaching experiments were recovered and subjected to different physico-chemical analyses including pH, EC (electrical conductivity), TDS (total dissolved solid), iron (Fe), and sulfate (SO₄²⁻) contents by using the “water analysis kit” (LAQUAtwin-pH-11, LAQUAtwin-EC-33, and TDS meter). The Fe and SO₄²⁻ concentrations were analyzed by using standard

analytical technique (Standard 2006) and atomic absorption spectroscopic analysis (AAS model No. ZEE nit 700P). The results of physico-chemical analysis of the aqueous leachates obtained from coal (TpHM1) and SPM samples at different leaching times and reaction temperatures are summarized in Tables 1 and 2, respectively.

2.4 Determination of pyrite oxidation kinetics

For evaluation of the pyrite oxidation kinetics, the residues obtained from the both leached-out coal (TpHM1) and SPM slurry were dried at 60 °C and the contents of pyritic sulfur were determined by using the ASTM Standard Methods D-2492 and D-3177 (Shimp et al. 1977). In many studies of sulfide oxidation kinetics, oxidation rates were measured by evaluation of production rates of Fe and SO₄²⁻, along with decrease in pH values. Therefore, the kinetic parameters of the oxidation reaction of CAPy and SPM (depyritisation) were derived from the contents of unreacted pyritic sulfur (FeS₂) present in both the residue samples taking them as reactants of the oxidation reaction. Based on the experimental conditions, SO₄²⁻ along with Fe³⁺ is produced by the oxidation of pyrite (FeS₂). The ratio of atomic percentage of Fe to S in pyrite is 2:1, and thus, the pyrite oxidation rate can be expressed as follows:

$$\frac{d[\text{Pyrite}]}{dt} = \frac{d[\text{SO}_4^{2-}]}{dt} = \frac{d(\text{Fe}^{3+} + \text{Fe}^{2+})}{dt} \quad (4)$$

Where, [pyrite], [SO₄²⁻], [Fe²⁺], and [Fe³⁺] denote the concentration changes of pyrite, SO₄²⁻, Fe²⁺, and Fe³⁺ in the reaction system, respectively; and ‘t’ is the reaction time. Hence, we have considered the variation of (wt%) pyritic sulfur (FeS₂) in the remaining coal and standard pyrite residues after aqueous leaching to evaluate the pyrite oxidation rates in both the aqueous leaching depyritization reaction. Aqueous depyritization experiments of coal (TpHM1) and SPM were performed maintaining the reaction parameters as mentioned in Table 3. The calculation for pseudo-first-order reaction kinetics was performed by using the following equations reported elsewhere (Baruah et al. 2006):

$$k = 1/t[\ln(C_0 - C_\infty)/(C_t - C_\infty)] \quad (5)$$

$$\ln[(C_0 - C_\infty)/(C_t - C_\infty)] = kt \quad (6)$$

Here, C₀, C_t, and C_∞ stand for the concentrations of pyritic sulfur in the leached-out residue samples of coal (TpHM1) and SPM at 0 (initial), t (at any time), and ∞ (overnight). The specific rate constants (k) were calculated for each temperature of 25, 50, 75, and 90 °C by applying standard regression method from the graph plotted between ln[(C₀—C_∞)/(C_t—C_∞)] as Y axis and time (hour) as X axis.

Table 1 Summary of the physico-chemical parameters of the aqueous leachates (filtrates) obtained from coal (TpHM1) leaching at different leaching times and reaction temperatures

Sl. No.	Reaction parameters		Stirring rate (rpm)	Filtrates of coal (TpHM1) slurry	pH	Fe (mg/L)	EC (Sm ⁻¹)	SO ₄ ²⁻ (mg/L)	TDS (mg/L)
	Time (hour)	Temperature (°C)							
1	0	25	300	CTpF-1	2.91	15.6	548.8	61.57	274.8
2	0.5			CTpF-2	2.98	25.0	409.5	18.36	198.5
3	1			CTpF-3	3.50	19.90	231.7	10.05	114.2
4	6			CTpF-4	3.34	13.25	314.0	40.70	154.3
5	8			CTpF-5	2.97	7.10	382.5	42.95	182.7
6	24			CTpF-6	2.58	20.9	1118.0	30.57	548.4
7	0	50	300	CTpF-7	2.82	15.6	652.3	43.11	308.2
8	0.5			CTpF-8	2.60	5.85	826.5	35.97	404.9
9	1			CTpF-9	2.64	13.7	877.2	12.62	426.5
10	6			CTpF-10	2.59	9.5	848.5	15.56	442.5
11	8			CTpF-11	2.72	13.7	607.1	27.04	295.8
12	24			CTpF-12	2.94	9.06	763.1	23.99	367.8
13	0	75	300	CTpF-13	2.68	15.6	679.1	96.02	328.4
14	0.5			CTpF-14	2.56	11.7	892.2	50.53	427.4
15	1			CTpF-15	2.78	18.9	528.8	56.52	255.5
16	6			CTpF-16	2.75	21.2	723.2	42.76	348.1
17	8			CTpF-17	2.66	15.7	1123.0	30.83	545.2
18	24			CTpF-18	2.61	16.7	1127.0	48.75	542.7
19	0	90	300	CTpF-19	2.83	15.6	578.8	44.04	280.9
20	0.5			CTpF-20	2.82	11.7	551.2	27.43	266.8
21	1			CTpF-21	2.70	14.8	692.9	42.66	336.4
22	6			CTpF-22	2.65	16.0	927.4	69.11	927.4
23	8			CTpF-23	2.70	14.9	878.2	83.31	878.2
24	24			CTpF-24	2.55	10.6	1264.0	37.29	1264.0

2.5 Analytical characterization techniques of the filtrates and residues

2.5.1 X-ray photo-electron spectroscopy

The nature of the chemical bonding and/or environment/compositions of the residue samples were evaluated by using X-ray photoelectron spectroscopy (XPS) analysis (Thermo Fisher Scientific ESCALAB Xi⁺). A spherical energy analyzer with an electromagnetic lens mode and an Al K α monochromatic X-ray source operating at 1486.6 eV was used to run the XPS analyzer. The constant analyzer energy was 100 eV and 50 eV for the survey spectrum and a high-resolution spectrum, respectively. To evaluate the extent of pyrite oxidation and acid formation, two sets of filtrate samples obtained from the controlled oxidation of coal and SPM samples were also subjected for XPS analysis. One set comprises of initial filtrates of coal (TpHM1) and SPM by simply mixing with distilled water at room temperature, without giving enough time for stirring (0 h, 25 °C) i.e., CTpF-1 and PyF-1 to the immediate effects. Another set contains filtrates of coal (TpHM1) and

SPM slurry, obtained after a leaching time of 24 h and at a temperature 90 °C i.e., CTpF-1 and CTpF-24. Filtrate samples to be analyzed by XPS were coated in a small glass slide (12 mm × 6 mm × 1 mm) and dried in a hot air oven (temperature 50 °C) to form a thick layer. This analysis was performed to find the impact of pyrite and other ferric ions along with the C-S bond in AMD generation. Moreover, in our study, XPS analysis gives a quantitative approach for comparing intensities of ferric and ferrous ions to determine the amount of active ions at the surface of the dissolved compounds present in the samples.

2.5.2 High resolution-transmission electron microscopic analysis (HR-TEM)

The nano- and micro-structural analysis of the two residues samples, i.e., CTpR-1 (0 h at 25 °C) and CTpR-24 (24 h at 90 °C), obtained from the coal (TpHM1) leaching experiments were evaluated by performing the HRTEM analysis (JEOL JEM-2100 Plus). Then, the TEM images were used

Table 2 Summary of the physico-chemical parameters of the aqueous leachates obtained from SPM leaching at different leaching times and reaction temperatures

Sl. No.	Reaction parameters		Stirring rate (rpm)	Filtrates of SPM slurry	pH	Fe (mg/L)	EC (Sm ⁻¹)	SO ₄ ²⁻ (mg/L)	TDS (mg/L)
	Time (hour)	Temperature (°C)							
1	0	25	300	PyF-1	4.40	10.95	78.98	62.71	37.99
2	0.5			PyF-2	5.14	0.97	84.25	60.15	39.58
3	1			PyF-3	6.16	0.05	96.01	66.72	44.18
4	6			PyF-4	6.28	0.03	114.0	66.69	52.60
5	8			PyF-5	6.10	0.28	108.6	68.36	50.41
6	24			PyF-6	6.03	0.09	124.1	75.12	102.2
7	0	50	300	PyF-7	4.30	10.95	74.84	56.14	34.17
8	0.5			PyF-8	5.66	0.76	93.5	65.84	43.86
9	1			PyF-9	6.21	0.26	95.24	67.78	45.85
10	6			PyF-10	6.01	0.04	225.5	74.30	105.2
11	8			PyF-11	6.33	0.03	239.0	79.20	112.2
12	24			PyF-12	5.90	0.12	343.7	96.83	157.5
13	0	75	300	PyF-13	5.07	10.95	64.89	55.61	30.49
14	0.5			PyF-14	5.51	1.13	104.2	67.67	48.67
15	1			PyF-15	6.43	0.55	106.5	75.95	55.43
16	6			PyF-16	6.50	0.20	295.0	81.40	138.7
17	8			PyF-17	6.15	0.19	274.5	83.69	128.1
18	24			PyF-18	6.65	0.08	463.7	98.89	211.4
19	0	90	300	PyF-19	4.49	10.95	100.2	66.05	45.51
20	0.5			PyF-20	6.22	0.94	111.4	72.94	52.57
21	1			PyF-21	5.38	0.47	118.6	75.83	57.50
22	6			PyF-22	6.43	0.12	282.6	84.31	132.2
23	8			PyF-23	5.22	1.50	758.5	139.50	358.8
24	24			PyF-24	6.62	0.17	575.7	105.56	271.2

for analyzing the presence of the nanoparticles and nano-structural features in the residual samples.

2.5.3 X-ray powder diffraction (P-XRD)

The mineralogy of raw coal (TpHM1), SPM, and two residue samples CTpR-1 (0 h at 25 °C) and CTpR-24 (24 h at 90 °C), obtained from the coal (TpHM1) were analyzed by using P-XRD (Model: Bruker D8 Advance) in the range of angle 5°–90° at a 1° per minute scan rate with Cu K-alpha radiation.

3 Results and discussion

3.1 Physico-chemical characteristics of the aqueous leachate samples (filtrates)

The physico-chemical parameters including pH, EC, TDS, and the Fe contents of the leachates/filtrates, that were obtained after aqueous leaching experiments of coal

(TpHM1) and SPM samples were measured and summarized in Table 1. The pH values of the coal leachates decrease gradually from initial stage of reaction to 24 h of leaching time at all the four temperatures (25, 50, 75, and 90 °C). The EC of the filtrates at same temperature and different reaction time shows a continuous increment, suggesting generation of dissolved ions in the solution on faster progress of the oxidation reaction. Similarly, the TDS values are found to be increased gradually with increase in the time period of leaching and leaching temperature (from 25 °C to 90 °C). In the initial stage of the reaction (0–1 h), the concentration of each component (Fe, SO₄²⁻, H⁺, etc.) changes rapidly and then tends to become stable with increase in the time period and temperature of leaching (see Tables 1 and 2). Moreover, the SO₄²⁻ content of the oxidation products in the filtrates also increases. As the reaction progressed, the pH value shows a decreasing trend for both coal (TpHM1) and SPM leaching reactions (Tables 1 and 2), indicating that pyrite oxidation involves acid production and oxidant consumption. The pH value

Table 3 Pyritic sulfur (FeS_2) analysis in the coal (TpHM1) residues and SPM residues at different temperature and time periods (wt %)

Sl. No.	Reaction parameters			Coal residues			SPM residues		
	Time (hour)	Temperature ($^{\circ}\text{C}$)	Stirring rate (rpm)	Sample code	FeS_2	FeS_2 dissolved	Sample codes	FeS_2	FeS_2 dissolved
1	0	25	300	CTpR-1	0.51	70.58	PyR-1	40.7	66.14
2	0.5			CTpR-2	0.5		PyR-2	40.69	
3	1			CTpR-3	0.48		PyR-3	40.69	
4	6			CTpR-4	0.31		PyR-4	40.64	
5	8			CTpR-5	0.23		PyR-5	40.6	
6	24			CTpR-6	0.15		PyR-6	13.78	
7	0	50	300	CTpR-7	0.51	72.54	PyR-7	40.7	66.19
8	0.5			CTpR-8	0.49		PyR-8	40.69	
9	1			CTpR-9	0.46		PyR-9	40.68	
10	6			CTpR-10	0.31		PyR-10	40.6	
11	8			CTpR-11	0.21		PyR-11	40.56	
12	24			CTpR-12	0.14		PyR-12	13.76	
13	0	75	300	CTpR-13	0.51	78.48	PyR-13	40.7	66.31
14	0.5			CTpR-14	0.48		PyR-14	40.68	
15	1			CTpR-15	0.47		PyR-15	40.66	
16	6			CTpR-16	0.28		PyR-16	40.59	
17	8			CTpR-17	0.18		PyR-17	40.49	
18	24			CTpR-18	0.11		PyR-18	13.71	
19	0	90	300	CTpR-19	0.51	80.39	PyR-19	40.7	66.83
20	0.5			CTpR-20	0.48		PyR-20	40.68	
21	1			CTpR-21	0.45		PyR-21	40.65	
22	6			CTpR-22	0.25		PyR-22	40.58	
23	8			CTpR-23	0.17		PyR-23	40.47	
24	24			CTpR-24	0.10		PyR-24	13.5	

initially increases and then decreases in the reaction system of aqueous leaching of both coal (TpHM1) and SPM samples. However, the pH for all the coal leachates are found to be relatively consistent around 2.90–2.55 over a temperature range of 25 to 90 $^{\circ}\text{C}$ (see Table 1). The pH of the coal leachate (CTpF-24) is found to be extremely acidic (2.55) after 24 h of leaching at 90 $^{\circ}\text{C}$, indicating the release of excessive H^+ ions.

The leachable level of Fe sharply decreases to 10.6 mg/L for coal filtrate CTpF-24 that is obtained after leaching at extreme condition of temperature and time (90 $^{\circ}\text{C}$, 24 h) (Table 1), towards highly acidic values (pH 2.55). From the results of physicochemical analysis of the filtrates of leaching experiments (Tables 1 and 2), it can be interpreted that at low pH conditions, Fe solubility in the filtrates increases, as the high concentration of protons (H^+) weaken the Fe-S bonds of pyrite facilitating the detachment of Fe from the surface lattice (Izquierdo and Querol 2012). Since oxidation of Fe^{2+} from FeS_2 triggers the release of Fe^{3+} , it can potentially be speculated that acidification stimulates dissolution kinetics. The concentrations of the total dissolved Fe particles (Fe^{2+} and Fe^{3+}) in the filtrates of coal (TpHM1)

slurry and SPM slurry show a significant difference for the two system. The emergence of Fe^{3+} is still inhibited as pyrite oxidation advances and dissolved Fe level rise because of the low pH values. However, even though dissolved Fe^{3+} ion is a potent oxidant during pyrite oxidation (Evangelou and Zhang 1995), its impacts on our studies may be overlooked. Tables 1 and 2 reflect that, the generated ion concentrations such as $\text{Fe}^{2+}/\text{Fe}^{3+}$ or SO_4^{2-} are higher in case of CAPy than that of SPM system; suggesting the presence of some other (excluding pyrite) dissolved Fe-containing minerals in the reaction system of coal. The information in Table 1 shows that the quantities of released ions (i.e., H^+ , Fe ions, and SO_4^{2-}) in the coal filtrates (TpHM1) are considerably higher than those of SPM filtrates (Table 2), which explains why the pH value of the SPM is quite higher and also suggests the presence of some other dissolved iron-containing minerals except pyrite in the reaction system of raw coal.

Furthermore, compared to SPM, the variation range for each component (Fe, SO_4^{2-} , H^+ , etc.) in the CAPy during coal (TpHM1) leaching is more severe. The SO_4^{2-} and TDS concentration values rise throughout the system as leaching time and temperature rise for both coal and SPM systems.

3.2 Results from the kinetics study

The pyritic sulfur (pyrite contents) remained in the residues of both coal (TpHM1) and SPM samples along with the amount of pyrite dissolved after aqueous leaching experiments are summarized in Table 3. The pseudo-unimolecular

Table 4 Kinetics parameters for aqueous oxidation of coal-associated pyrite (CAPy) and standard mineral pyrite (SPM)

Sample	Temperature (K)	Rate constants (h ⁻¹)	Activation energy (kJ mol ⁻¹)	Frequency factor (h ⁻¹)
Coal (TpHM1)	298	0.1779	2.124	0.417
	323	0.1873		
	343	0.1992		
	363	0.2077		
Standard Mineral pyrite (SPM)	298	0.0004	10.838	0.034
	323	0.0007		
	343	0.0008		
	363	0.0009		

kinetic parameters such as rate constant, activation energy, and frequency factor measured for both the reactions are depicted in Table 4.

The coal (TpHM1) and SPM samples during overnight (i.e., 24 h) aqueous leaching reaction undergo oxidation and show pyritic sulfur removal (depyritization) up to 80.39% and 66.31% at 90 °C for CAPy in coal and the SPM samples, respectively. Thus, the removal of pyritic sulfur by ambient aqueous oxidation increases with the rise in temperature of the reaction systems (Table 3). The oxidation rate of pyrite is found to be significantly higher in case of CAPy in coal (TpHM1) than that of SPM under the same set of conditions. The reaction kinetics of oxidation of CAPy in coal (TpHM1) and SPM that are derived from the above-mentioned experimental data and equations (see Table 3) follows pseudo-first-order reaction kinetics. The linear type of plot obtained is in support with the pseudo-first-order reaction kinetics (Fig. 1a and c). Table 4 represents the specific rate constants, activation energy, and frequency factor at different chosen temperatures for both CAPy in TpHM1 and the SPM. On comparing the Arrhenius equation;

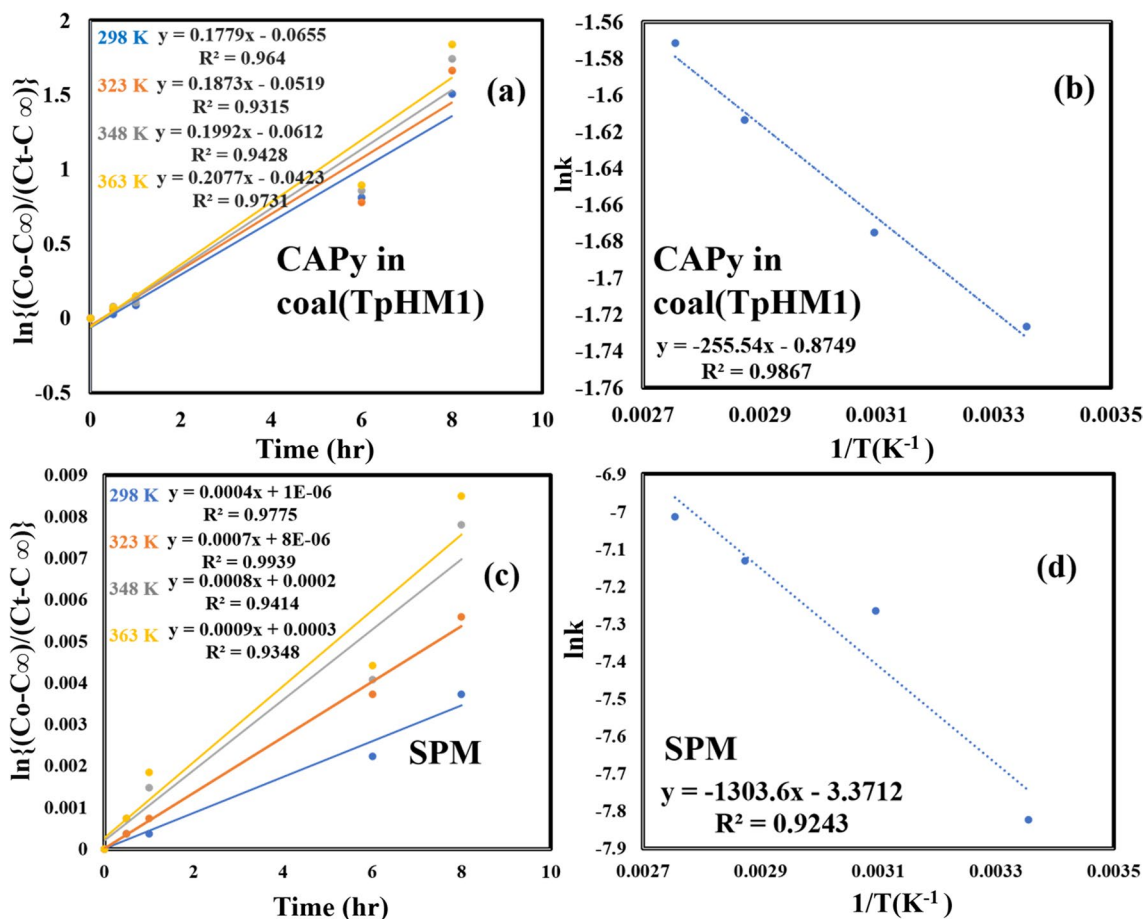


Fig. 1 Pseudo-unimolecular kinetic plots for pyritic sulfur oxidation of **a** CAPy in coal (TpHM1) and **c** SPM sample in aqueous leaching experiments at different time periods; **b** Arrhenius plot for aqueous pyritic sulfur oxidation in **b** CAPy in coal (TpHM1) and **d** SPM sample

$$\ln k = \ln A - \frac{E_a}{RT} \quad (7)$$

the derived equation from the plots between “1/T vs lnk” (see Fig. 1b and d) can be written as:

$$\ln k_{\text{CAPy}} = -\frac{255.4}{T} - 0.8749 \quad (8)$$

$$\ln k_{\text{SPM}} = -\frac{1303.6}{T} - 3.3712 \quad (9)$$

where, E_a is the activation energy of the reaction and denotes an energy barrier that the reactants must negotiate in order to proceed the reaction to proceed, and 'A' is a "pre-exponential" or frequency component associated with the geometry of the activated complex. From the slopes of Eqs. (8) and (9), the activation energies of $2.124 \text{ kJ mol}^{-1}$ and $10.838 \text{ kJ mol}^{-1}$ for the depyritisation of coal (TpHM1) and SPM, respectively, are calculated for aqueous media. The intercepts of the plots yield 0.417 and 0.034 s^{-1} as the frequency factor (A) of the ambient atmospheric oxidation reaction of CAPy and SPM, respectively. The rate constants are found to be increased with the rise in temperature of the reacting systems for both the samples. But the rate constants of the CAPy dissolution are much higher than that of SPM. This is in accordance with the usual temperature dependence of the rate of a chemical reaction. Differences in the calculated activation energies and rate constants values of pyrite oxidation associated with CAPy in coal (TpHM1) and SPM may be because of the inherently found FeS_2 in coal (TpHM1). Hence, CAPy is much prone to atmospheric oxidation than that of SPM. Compared to the SPM, the oxidation process and mechanism of inherent CAPy is more complex and affected by many factors. The various compositions of CAPy can also lead to different oxidation processes in coal leaching reactions. The observation is also well-supported through combination of analytical and mineralogical characterizations of the samples.

3.3 Observations from analytical characterizations

3.3.1 X-ray photoelectronic spectroscopy

Figures 2a–d depict the XPS spectral analysis for $\text{Fe}2p_{3/2}$ and $\text{S}2p$ peaks of the filtrates obtained from SPM slurry on oxidation at $25 \text{ }^\circ\text{C}$ for 0 h (PyF-1) and $90 \text{ }^\circ\text{C}$ for 24 h (PyF-24). These spectras demonstrate the chemical states of Fe (oxidized or unoxidized) and sulfur (oxidized or unoxidized) containing compounds generated during controlled oxidation reaction. The deconvoluted XPS spectra of PyF-1 contains two doublets, with maxima at 165.62 and 168.3 eV which are assigned to thiosulfate ($\text{S}_2\text{O}_3^{2-}$) and sulfate (SO_4^{2-}) on

surface of the pyrite particles. PyF-1 also have another peak at 162.41 eV corresponding to a low weight percentage of the persulfate anion (S_2^{2-}). In contrast, deconvoluted $\text{S}2p$ XPS spectra of PyF-24 reveals only oxidized species such as SO_4^{2-} , which suggests the complete oxidation of pyrite at 169.86 – 168.32 eV and also a very low intensity $\text{S}_2\text{O}_3^{2-}$ at 166.4 eV . Detection of $\text{S}_2\text{O}_3^{2-}$ suggests seven electrons transfer process during pyrite oxidation. The weight percentage of $\text{S}_2\text{O}_3^{2-}$ peaks of both PyF-1 and PyF-24 reveals the production of the oxidized products dominating over the unoxidized products with the progress of the reaction. PyF-24 spectra shows that thiosulfate is only present at the initial stage of pyrite oxidation, thereby indicating that thiosulfate rapidly converts to sulfate. XPS $\text{Fe} 2p_{3/2}$ spectra of the PyF-1 contains peaks at 709.14 eV assigned to Fe^{2+} -O type species (Eggleston et al. 1996). PyF-1 shows peaks at 724.2 and 728.03 eV corresponding to the $\text{Fe}2p_{1/2}$ state indicating the presence of Fe^{3+} -O with a very low intensity. Peak value at 714.25 – 715.70 eV is corresponds to Fe^{2+} -S (Li et al. 2019). After 24 h reaction in aqueous media at $90 \text{ }^\circ\text{C}$; one of the fitted peaks at 709.14 eV , which (Fig. 2b) corresponds to Fe^{2+} in Fe–O is replaced possibly by Fe^{3+} -O (711.11 eV) due to incipient oxidation in PyF-24 (Fig. 2d). Moreover, one satellite peak of $\text{Fe} 2p_{1/2}$ in PyF-1 is replaced by a broader peak of Fe^{3+} at 725.04 eV in PyF-24. From the literature, it is known that the peak at 711.1 eV can be assigned to the Fe^{3+} in oxides or oxyhydroxides (Li et al. 2019). XPS $\text{Fe}2p_{3/2}$ spectra of coal filtrates (CTpF-1 and CTpF-24) in Fig. 2e, f were deconvoluted into three peaks at binding energies of 715.09 (Fe^{2+} -S), 711.44 (Fe^{3+} -S), and 709.6 (Fe^{3+} -S) eV. The $\text{S}2p$ peak of CTpF-1 (Fig. 2e) can be deconvoluted into three peaks, with binding energies 169.63 , 168.41 are responsible for SO_4^{2-} and 165.45 eV is responsible for $\text{S}_2\text{O}_3^{2-}$ group respectively. $\text{S}2p$ spectra of CTpF-24 contains peak fitting at binding energies 169.57 , 168.78 , and 167.99 eV that are characteristics peak for SO_4^{2-} group. Both the $\text{S}2p$ XPS spectras of the coal filtrate (i.e., CTpF-1 & CTpF-24) samples do not have an exact fit at 162.41 eV , which indicate that coal during pyrite oxidation forms oxidized S-compounds instead of persulfate anion species (S_2^{2-}). The weight percent ratio of the $\text{Fe}^{3+}/\text{Fe}^{2+}$ and the S/Fe derived from the $\text{Fe}2p$ and $\text{S} 2p$ XPS spectral analysis of the coal and SPM filtrate samples at different oxidation intervals (Table 5) show an increasing trend over oxidation time for both coal and SPM system, but variation is much more significant in the case of raw coal system.

3.3.2 Transmission electron microscopic (TEM) analysis of the aqueous residues

Figures 3 and 4 represent the HRTEM image of two coal slurry residue samples CTpR-1 (0 h at $25 \text{ }^\circ\text{C}$) and CTpR-24 (24 h at $90 \text{ }^\circ\text{C}$) along with their EDS. These images reveal the presence of sub-micron minerals dispersed in the coal

Fig. 2 XPS analysis showing the high resolution and deconvoluted spectra of S 2p **a**, PyF-1, **b** PyF-24; Fe 2p **c** PyF-1 **d** PyF-24; S2p **e** CTpF-1 **f** CTpF-24 samples and Fe 2p **g** CTpF-1 **h** CTpF-24 sample

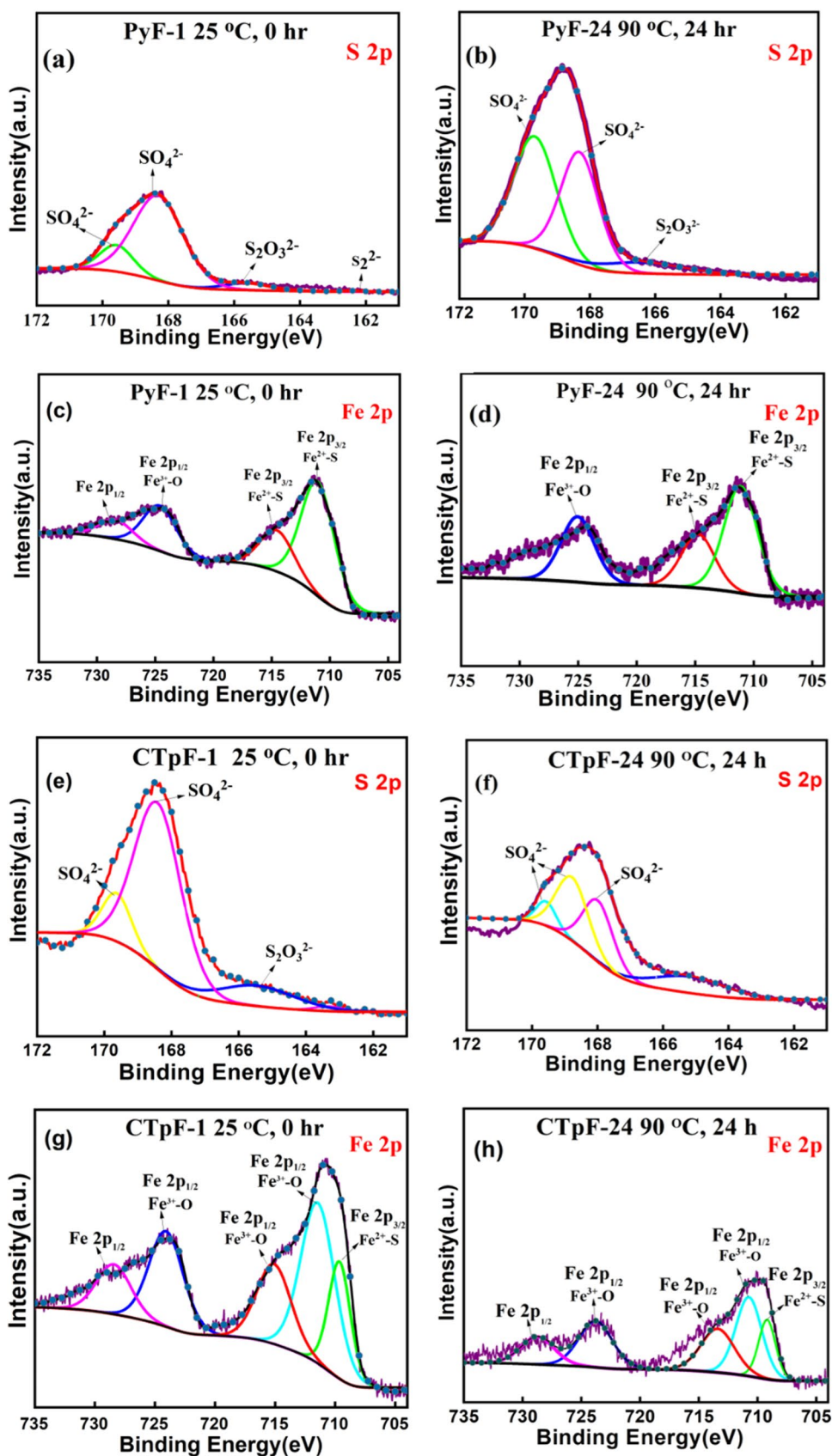
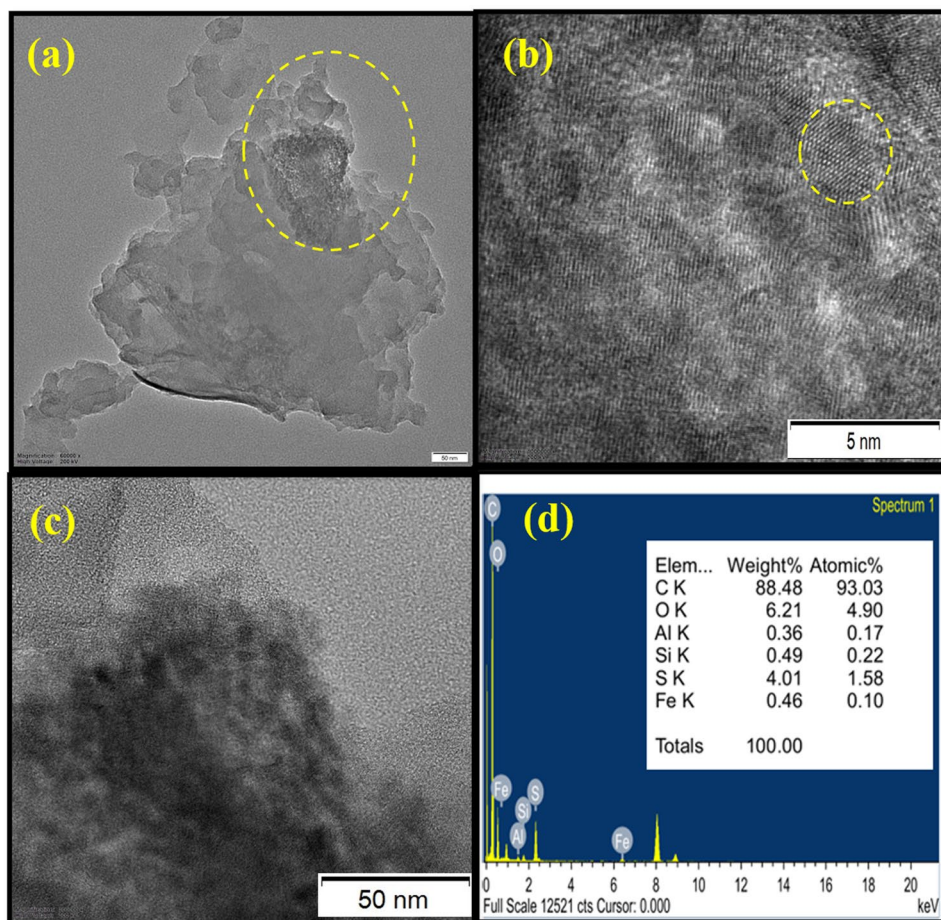


Table 5 Calculation of Fe³⁺:Fe²⁺ and Fe:S ratios from the XPS deconvoluted spectra for the residue samples derived from SPM and coal after aqueous leaching/oxidation reaction at 25 and 90 °C

Raw sample	Analyzed filtrate	Time (h)	Temperature (°C)	Atomic (wt%)				Atomic weight ratio	
				Total S	Total Fe	Fe ³⁺	Fe ²⁺	Fe:S	Fe ³⁺ :Fe ²⁺
Standard pyrite	PyF-1	0	25	4.04	2.23	29.75	6.350	0.552	4.685
	PyF-24	24	90	15.66	2.59	72.78	27.23	0.850	6.040
Coal (TpHM1)	CTpF-1	0	25	6.12	3.30	31.73	33.52	0.539	0.946
	CTpF-24	24	90	3.52	1.72	63.36	17.06	0.488	3.710

Fig. 3 HRTEM image analysis of CTpR-1 (residue of coal slurry obtained on leaching at 25 °C for 0 h leaching); **a** Indicating the presence of Fe-hydroxide/oxides in coal residue, **b** Fe-nanoparticles observed as singular nano-hematite, **c** Disseminated Al and Si can be suspected for the existence of Kaolinite and Quartz in CTpR-1 **d** EDS spectrometry of the sample obtained from TEM analysis



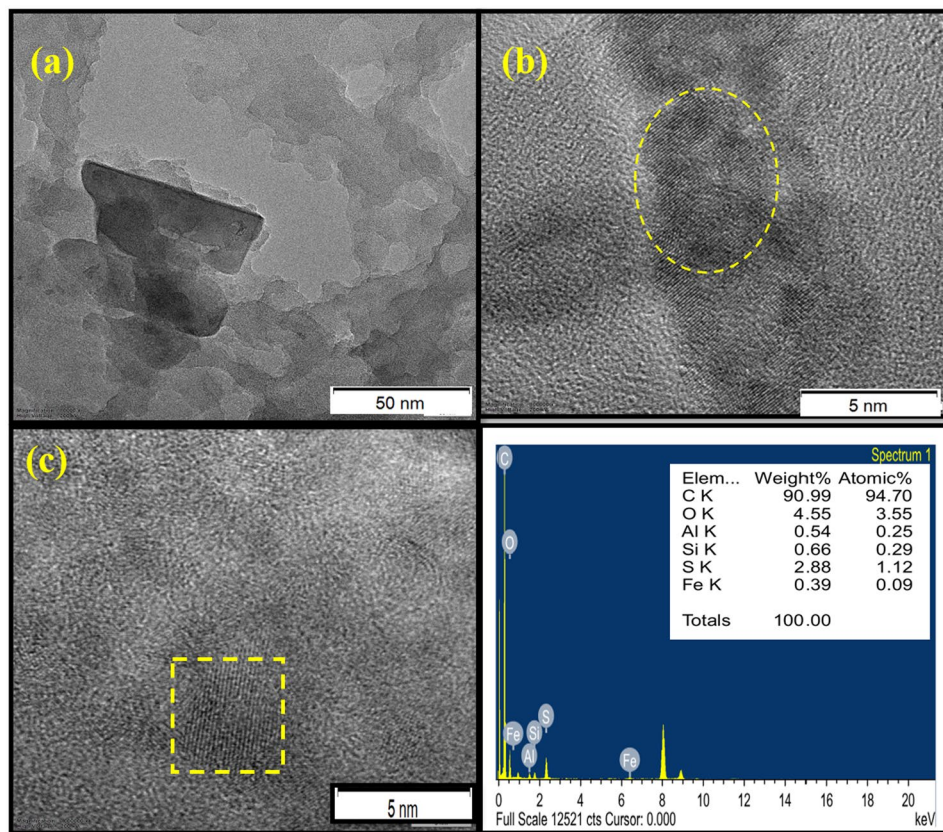
samples. TEM analysis of CTpR-1 and CTpR-24 indicate the presence of some Fe-nanocomposites (nano-hematite) (Figs. 3a and 4a), which is in consistent with the results reported by Dutta et al. (2017). Jarosite in combination with kaolinite containing high concentrations of Al and Si can be suspected to be disseminated in agglomerated form in CTpR-1 and CTpR-24 coal residues (Figs. 3a and 4a). From the evidence of Si and O in EDS spectrometry (Figs. 3d and 4d), Quartz is also suspected in the coal residues. The surface-topography, microstructural, and the elemental compositions of CTpR-1 and CTpR-24 confirmed that, in the progress of the oxidation reaction, the iron and sulfide

components in minerals vanish (on comparing the EDS results of CTpR-1 and CTpR-24). It can be validated from this characterization study that with increasing oxidation reaction parameters, the extent of substituting the pyrite lattice by mineral impurity dominates, thus causing crystal defects.

3.3.3 P-XRD analysis

In Fig. 5, the XRD spectra is shown to depict the crystalline properties of SPM, raw coal (TpHM1), and the coal residues CTpR-1(0 h, 25 °C) and CTpR-24 (24 h, 90 °C). The SPM

Fig. 4 HRTEM image analysis of CTpR-24 (residue of coal slurry obtained by leaching at 24 h, 90 °C.). **a** Sub-micron mineral matters composed of Al, Si and Fe in coal residue. **b-c** Agglomerated forms of nano-particles of these minerals containing disseminated Al, Si and Fe in high concentration and **d** EDS spectrometry of the sample obtained from TEM analysis



demonstrates a good crystallinity and the peaks at 33.1°, 37.1°, 40.8°, 47.47°, and 56.3° can be well indexed to the (200), (210), (211), (220), and (311) planes of Pyrite (FeS_2), respectively (Li et al. 2019). The XRD result show distinctive peaks that corresponds to pyrite without any other mineral impurity. The XRD pattern of raw and leached coal residues show a wide protrusion in the range of 5–35° without a clear peak, which is perceivable in the amorphous structure of coal. From the XRD results, Gypsum ($\text{CaSO}_4 \cdot 2\text{H}_2\text{O}$), Quartz (SiO_2), Kaolinite ($\text{Al}_2\text{O}_3 \cdot 2\text{SiO}_2 \cdot 2\text{H}_2\text{O}$) and a minor proportion of Pyrite (FeS_2) are evident as prime mineral matters incorporated in Coal. CTpR-1 According to Pine-town et al. (2007) and Saikia et al. (2014); the presence of these minerals might be the cause of interplay among organically-associated Ca, Al, N, and organic-S released from the macerals and oxidation of the organic matter during low-temperature ashing. A significant amount of minerals such as Gypsum (G) and Quartz (Q) are present in the raw coal samples, which are also remained after leaching experiment, but get significantly broadened on increasing leaching time and temperature as shown in the XRD peaks of CTpR-1 and CTpR-24. However, peak intensity corresponding to the Pyrite (Py) mineral is almost trivial on progress of the oxidation reaction.

3.4 Characteristics of CAPy and SPM samples and their implications in depyritization reaction

The distribution of pyrite in the coal sample displays a notable diversity, with different mineral composition and crystal structure as compared to SPM (Saikia et al. 2014). The study on environmental assessment and nano-mineralogical characterization of Tirap coal by using ^{57}Fe Mossbauer spectra and XRD analysis reported the evidence of different iron-containing minerals in coal in addition to pyrite (Dutta et al. 2017). The nano-mineralogical analysis of the coal also reveals the presence of Si minerals like Kaolinite [$\text{Al}_2\text{Si}_2\text{O}_5(\text{OH})_4$], Quartz (SiO_2). In addition to pyrite, the common Fe-containing minerals in coal seams include Hematite (Fe_2O_3), Ankerite ($\text{Ca}(\text{Mg}, \text{Fe})(\text{CO}_3)_2$), Illite ($\text{K}, \text{H}_2\text{O}$) ($\text{Al}, \text{Mg}, \text{Fe})_2(\text{Si}, \text{Al})_4\text{O}_{10}(\text{OH})_2(\text{H}_2\text{O})$, (Dutta et al. 2017). These minerals are more easily dissolved in acidic solutions, resulting in a higher Fe^{2+} concentration increase. Thus reaction rate of the inherited coal pyrite is higher than that of the SPM system in the initial stage. From P- XRD and TEM analysis, it is noticed that the oxidation products of Pyrite, i.e., Jarosite and Iron sulfate, also play a key role in the rate of pyrite oxidation in CAPy (Saikia et al. 2014). Moreover, the abnormality in the pyrite dissolution (depyritization) reaction by atmospheric oxidation in CAPy in contrast to

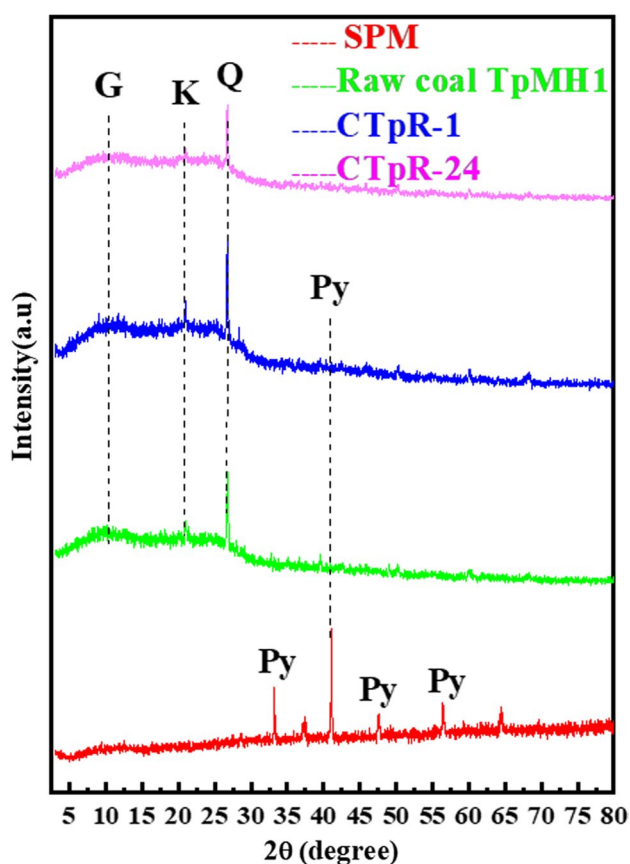


Fig. 5 XRD analysis of coal residues; CTpR-1(0 h at 25 °C) and CTpR-24 (0 h at 90 °C) along with SPM and raw coal (TpMH1) for observing the modifications in mineral phases of the processed coal samples over the raw sample. P-XRD analysis indicates the presence of significant mineral phases such as Gypsum (G), Kaolinite (K) and Quartz (Q) with their varying intensity

SPM can be linked to the formation process of pyrite in coal seams. The formation process of pyrite involves two evolution modes, direct precipitation and genesis (Tang and Ren 1996). Lattice substitution and isomorphism can allow impurity elements to infiltrate the lattice during this process. Potentially toxic trace elements present in coal in aggregated form can occupy some of the lattice sites of the pyrite crystal lattice, which may lead to crystal defects (Liu et al. 1998), and eventually catalyzing the dissolution process of pyrite. The XPS and TEM analysis supports strongly the influence of Hematite and Alumina on the overall dynamics of pyrite oxidation because of their ability to change the solution chemistry and alter the electrochemical properties of pyrite itself (Tabelin et al. 2017).

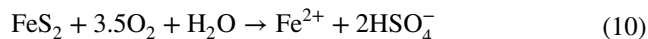
In addition, the organic matter in the coal body can also affect the oxidation process of pyrite. CAPy formation is more visibly impacted by organic materials than mineral-pyrite. In that context, humic acids with active groups such as carboxyl and hydroxyl functional groups are abundant in

coal seams and have significant adsorption, complexation, and ion exchange properties (Illés and Tombácz 2003; Zheng et al. 2018). Moreover, the interface interaction between $\text{Fe}^{3+}/\text{O}_2$ and pyrite can be slowed down or even prevented by the adsorption of humic acid on the pyrite surface (Zheng et al. 2018). Hence, pyrite can therefore interact with clay minerals and organic material in coal bodies, which further alters its electrochemical characteristics and contributes to the overall oxidation experiment. In view of that, the north-east Indian coals have unusual physico-chemical characteristic such as high organic sulfur (75%–90% of the total sulfur), with majority of the S organically bound (Saikia et al. 2014). Hence, the studied coal sample (TpMH1) contain organic sulfur, which primarily takes the form of sulfoxides and thiophene during the oxidation reaction and eventually contribute to generation of acids (Saikia et al. 2014).

3.5 Comparison of theoretically and experimentally (aqueous leaching of coal) determined pH values of pyrite oxidation reaction

3.5.1 Complete oxidation reaction of standard pyrite mineral (SPM)

Pyrite oxidation in the presence of water and air leads to the formation of acid (H^+), sulfates (SO_4^{2-}), and aqueous Fe (II) ions:



Ideally, the ratio of total iron:proton:sulfate derived from the balanced chemical reaction should be 1:2:2. This molar ratio of iron:protons:sulfate derived from the stoichiometry of the overall reaction reflects complete oxidation of sulfide mineral pyrite (FeS_2) to sulfate (SO_4^{2-}), if the iron and sulfur are properly counted, i.e., if no sulfate minerals or iron oxyhydroxide minerals precipitate before sampling the water (Druschel et al. 2004). In this study, the approximate value of pH as a measure of H^+ ion generation potential during the pyrite dissolution/oxidation process is calculated. Here, stoichiometry of Eq. (10) is considered as the main mechanistic step for H^+ ion generation during pyrite oxidation.

For this purpose, we have considered the pyritic sulfur content (%w/w) obtained after aqueous leaching of Tirap coal (TpMH1) at 25 °C with 0 h of stirring. From Table 3, the variation of % pyritic sulfur (FeS_2) in the coal residue CTpR-1) (0 h at 25 °C) is found to be 0.51%. Using the stoichiometric ratio derived from the balanced chemical reaction (Eq. 10), pH value for the reaction of 0.51% pyrite (w/w) with H_2O can be calculated theoretically. Thus, one mole of FeS_2 reacts with one mole of H_2O to form two moles of H^+ (considering complete dissociation of H_2SO_4) 0.51% w/w solution of pyrite contain 0.51 g of pyrite in 100 g coal. As

we have taken 5 g of coal sample in 0.1 L of H₂O during the experiment, the pyrite content present can be calculated as 0.0255 g. Here, we have considered density of subbituminous coal as 1346 kg/m³ in our calculation (Congo et al. 2023). The calculated values of number of moles and volume of reactants and products of the stoichiometric oxidation reaction are given in Table 6, respectively.

Hence, concentration of H⁺ ions in terms of Molarity (mol/L):

$$\text{Molarity} = \frac{\text{mole of hydrogenion}}{\text{total volume}} = \frac{0.000425 \text{ mol}}{0.1037 \text{ L}} = 0.04098 \text{ M} \quad (11)$$

From the above data (for Eq. 10), pH as a measure of hydrogen ion (H⁺) concentration is calculated to be 1.38. The filtrate CTpF-1 is the respective filtrate of coal residue CTpR-1 and the experimental pH value is observed to be 2.91 (Table 1), which is higher than the theoretically calculated pH value. This outcome suggests that there are some agents in raw coal (TpHM1) that are consuming the acid-causing materials during pyrite oxidation/dissolution. The deviation in the experimental pH value from the theoretical value may also be attributed due to dissolution and alteration of various minerals that can contribute to the neutralization of acid; because of this, all the H⁺ ions may not be included in the pH contribution. Various minerals present in earth crust can neutralize acidic drainage such as, (i) Ca- and Mg-bearing carbonates; (ii) oxides and hydroxides of Ca, Mg, and Al; (iii) soluble, nonresistant silicate minerals; and (iv) phosphates (primarily apatite). An alternative definition of alkalinity for most near surface waters can be represented as the summation of [H⁺] + [OH⁻] + [HCO³⁻] + 2[CO₃²⁻] + [NH₃] + [HS⁻] + 2[S₂⁻] + [HSiO₃⁻] + 2[SiO₃²⁻] + [B(OH)₄⁻] - [H₃PO₄] + [HPO₄²⁻] + 2[PO₄³⁻] (Sherlock et al. 1995). Alkalinity may include caustic alkalinity, carbonate alkalinity, and alkalinity (Abraitis et al. 2004; Druschel et al. 2004).

As noted above, the ratio of iron:proton:sulfate predicted for the complete oxidation of pyrite to sulfuric acid is 1:2:2. Due to the difficulties of properly defining total H⁺ released and contributing to acidity practically, deviation of this value may occur from theoretical value (Druschel et al. 2004). This is because of (i) incomplete reoxidation of Fe²⁺ to Fe³⁺, (ii) Incomplete oxidation of the pyritic sulfide to S₈ or sulfoxy anion which is less oxidized than SO₄²⁻, and (iii) Precipitation of iron oxyhydroxide (Ferric) minerals.

4 Summary

This novel study conducts the ambient atmospheric pyrite oxidation experiments on the Tirap coal (TpHM1) and standard pyrite mineral (SPM) in a temperature and time-controlled environment without the addition of any oxidizer. From the results of physicochemical analysis of the filtrates of leaching experiments, it is observed that at low pH conditions, Fe solubility in the filtrates increases as the high concentration of protons (H⁺) weaken the Fe-S bonds of pyrite thus facilitating the detachment of Fe³⁺ from the surface lattice. Since oxidation of Fe²⁺ from FeS₂ triggers the release of Fe³⁺, it can potentially be speculated that acidification stimulates dissolution kinetics. The emergence of Fe³⁺ is still inhibited as pyrite oxidation advances and dissolved Fe³⁺ level rises because of the low pH values. Moreover, under the same conditions, the altering trend in each component in the reaction system of coal (TpHM1) is higher than that of SPM. Moreover, the oxidation rate of coal-associated pyrite (CAPy) seems to be higher than that of SPM in the initial reaction. The generated ion concentrations such as Fe²⁺/Fe³⁺ or SO₄²⁻ are higher in case of CAPy than that of SPM system; highlighting the role of some other Fe-containing minerals except pyrite to be dissolved in the reaction system. Nano-mineralogical characterization reveals the existence of silicate minerals such as Kaolinite and Quartz. The most frequent Fe-containing minerals encountered in coal sample, alongside Pyrite, are Hematite, Ankerite, and Illite. These minerals are more readily dissolved in acidic solutions and the increasing concentration of Fe²⁺ contributes to higher initial reaction rate of the coal-pyrite than that of SPM. A significant role in pyrite oxidation in coal is also played by the oxidation products of pyrite, that produce Jarosite and Iron sulfate. All of these additional factors somewhat affect the overall dynamics of the CAPy dissolution and eventually alter the depyritization rate in coal systems. Additionally, the experimental pH value of the CTpF-1 (0 h at 25 °C of leaching), is 2.91, which is considerably higher than the theoretically derived pH value of 1.38, indicating the dissolution and transformation of various alkalinity producing minerals that help enabling neutralization of acid and suggests that all of the liberated protons may not be included in the pH contribution during leaching. In summary, the experimental oxidation of coal-associated pyrite (CAPy) occurs rapidly due to

Table 6 Theoretically calculated possible pH value obtained by aqueous leaching of coal (with 0.51% pyritic sulfur content) (CTpR-1)

Mass of FeS ₂ reacted (g)	Molecular weight of FeS ₂ (g/mol)	Moles of		Volume (L)		Total solution volume (L)
		FeS ₂ reacts	H ⁺ ions form	Coal	H ₂ O	
0.0255	120	0.0002125	0.000425	0.003714	0.1	0.1037

variations in the mineral distribution and composition, trace elements, crystal structure, and organic components compared to that of standard mineral-pyrite. Moreover, various oxidation products may also result from the varied geochemical compositions and environment of the CAPy in coal and hence the understanding of CAPy dissolution and oxidation process is not simple. Further research and depth review is required to comprehend the dynamics of pyrite oxidation, to clarify the nature of pH dependency in toxic and anoxic systems and AMD production in the natural environment. Thus, it is necessary to thoroughly investigate the oxidation process of CAPy under the influence of diverse situations to appropriately prevent coal spontaneous combustion and the problem of acid mine drainage.

Acknowledgements Authors express thanks to the Director, CSIR-NEIST for the permission to conduct the study. The authors are also thankful to Ministry of Earth Science (Govt. of India) (GPP-0364).

Declarations

Conflict of interest The authors declare that they have no known competing financial interests or personal relationships that could have appeared to influence the work reported in this paper.

Open Access This article is licensed under a Creative Commons Attribution 4.0 International License, which permits use, sharing, adaptation, distribution and reproduction in any medium or format, as long as you give appropriate credit to the original author(s) and the source, provide a link to the Creative Commons licence, and indicate if changes were made. The images or other third party material in this article are included in the article's Creative Commons licence, unless indicated otherwise in a credit line to the material. If material is not included in the article's Creative Commons licence and your intended use is not permitted by statutory regulation or exceeds the permitted use, you will need to obtain permission directly from the copyright holder. To view a copy of this licence, visit <http://creativecommons.org/licenses/by/4.0/>.

References

- Abratis P, Patrick R, Kelsall G, Vaughan D (2004) Acid leaching and dissolution of major sulphide ore minerals: processes and galvanic effects in complex systems. *Mineral Mag* 68:343–351
- Aller RC, Rude PD (1988) Complete oxidation of solid phase sulfides by manganese and bacteria in anoxic marine sediments. *Geochim Cosmochim Acta* 52:751–765
- Baruah B, Khare P (2010) Mobility of trace and potentially harmful elements in the environment from high sulfur Indian coal mines. *Appl Geochem* 25:1621–1631
- Baruah BP, Saikia BK, Kotoky P, Rao PG (2006) Aqueous leaching on high sulfur sub-bituminous coals, in Assam, India. *Energy Fuels* 20:1550–1555
- Chen P, Chen W (1986) Study on the distribution characteristics of sulphur in Chinese coals. *Fuel* 65:1305–1309
- Congo T, Rodrigues S, Esterle J, Steel K, Maranha S (2023) Before and after: a visual glimpse into the coking behaviour of coal macerals. *Fuel* 343:127979
- Druschel GK, Baker BJ, Gihring TM, Banfield JF (2004) Acid mine drainage biogeochemistry at Iron Mountain, California. *Geochim Trans* 5:1–20
- Dutta M, Saikia J, Taffarel SR, Waanders FB, De Medeiros D, Cutruneo CM, Silva LF, Saikia BK (2017) Environmental assessment and nano-mineralogical characterization of coal, overburden and sediment from Indian coal mining acid drainage. *Geosci Front* 8:1285–1297
- Eggleston CM, Ehrhardt J-J, Stumm W (1996) Surface structural controls on pyrite oxidation kinetics: an XPS-UPS, STM, and modeling study. *Am Miner* 81:1036–1056
- Equenuddin SM (2010) Controls of coal and overburden on acid mine drainage and metal mobilization at Makum coalfield. IIT Kharagpur, Assam
- Evangelou VP, Zhang Y (1995) A review: pyrite oxidation mechanisms and acid mine drainage prevention. *Crit Rev Environ Sci Technol* 25:141–199
- Illés E, Tombácz E (2003) The role of variable surface charge and surface complexation in the adsorption of humic acid on magnetite. *Colloids Surf, A* 230:99–109
- Izquierdo M, Querol X (2012) Leaching behaviour of elements from coal combustion fly ash: an overview. *Int J Coal Geol* 94:54–66
- Li L, Ma P, Hussain S, Jia L, Lin D, Yin X, Lin Y, Cheng Z, Wang L (2019) FeS₂/carbon hybrids on carbon cloth: a highly efficient and stable counter electrode for dye-sensitized solar cells. *Sustain Energy Fuels* 3:1749–1756
- Liu C, Li S, Qiao Q et al (1998) Management of spontaneous combustion in coal mine waste tips in China. *Water Air Soil Pollut* 103:441–444
- Ma M, Wang W, Zhang K (2022) Occurrence characteristics of fine-grained pyrite in coal and its scaling effect on flotation desulfurization. *ACS Omega* 7:42467–42481
- Ma M, Wang W, Zhang K, Shi Z (2023) Experimental study on the oxidation reaction of coal-pyrite and mineral-pyrite with the participation of Fe(III) and bacteria under acidic conditions. *Energies* 16:3588
- Pinetown KL, Ward CR, Van der Westhuizen W (2007) Quantitative evaluation of minerals in coal deposits in the Witbank and Highveld Coalfields, and the potential impact on acid mine drainage. *Int J Coal Geol* 70:166–183
- Rickard D, Musmann M, Steadman JA (2017) Sedimentary sulfides. *Elements* 13:117–122
- Saikia BK, Ward CR, Oliveira ML, Hower JC, Baruah BP, Braga M, Silva LF (2014) Geochemistry and nano-mineralogy of two medium-sulfur northeast Indian coals. *Int J Coal Geol* 121:26–34
- Saikia BK, Khound K, Sahu OP, Baruah BP (2015) Feasibility studies on cleaning of high sulfur coals by using ionic liquids. *Int J Coal Sci Technol* 2:202–210
- Saikia BK, Saikia A, Choudhury R, Xie P, Liu J, Das T, Dekaboruah HP (2016) Elemental geochemistry and mineralogy of coals and associated coal mine overburden from Makum coalfield (North-east India). *Environ Earth Sci* 75:1–21
- Sherlock E, Lawrence R, Poulin R (1995) On the neutralization of acid rock drainage by carbonate and silicate minerals. *Environ Geol* 25:43–54
- Shimp N, Kuhn J, Helfinstine R, (1977) Determination of forms of sulfur in coal. [Evaluation of ASTM Standard Methods D-2492 and D-3177]. *Energy Sources*; (United States) 3.
- Standard I (2006) Methods of sampling and test (physical and chemical) for water and wastewater. IS. Search in.
- Tabelin CB, Veerawattananun S, Ito M, Hiroyoshi N, Igarashi T (2017) Pyrite oxidation in the presence of hematite and alumina: I. Batch leaching experiments and kinetic modeling calculations. *Sci Total Environ* 580:687–698
- Tang Y, Ren D (1996) The genesis of pyrites in coal. *Geol Rev* 42:64–70

Wang W, Sang S, Bian Z, Duan P, Qian F, Lei S, Qin Y (2016) Fine-grained pyrite in some Chinese coals. *Energy Explor Exploit* 34:543–560

Zhao Z, Peng S, Ma C, Yu C, Wu D (2022) Redox behavior of secondary solid iron species and the corresponding effects on hydroxyl radical generation during the pyrite oxidation process. *Environ Sci Technol* 56:12635–12644

Zheng Z, Zheng Y, Tian X, Yang Z, Jiang Y, Zhao F (2018) Interactions between iron mineral-humic complexes and hexavalent chromium and the corresponding bio-effects. *Environ Pollut* 241:265–271

Publisher's Note Springer Nature remains neutral with regard to jurisdictional claims in published maps and institutional affiliations.